World Academy of Science, Engineering and Technology
International Journal of Mechanical and Mechatronics Engineering
Vol:16, No:8, 2022

Structural Performance Evaluation of Electronic Road Sign Panels Reflecting Damage Scenarios

Junwon Seo, Bipin Adhikari, Euiseok Jeong

Abstract**—**This paper is intended to evaluate the structural performance of welded electronic road signs under various damage scenarios (DSs) using a finite element (FE) model calibrated with full-scale ultimate load testing results. The tested electronic road sign specimen was built with a back skin made of 5052 aluminum and two channels and a frame made of 6061 aluminum, where the back skin was connected to the frame by welding. The size of the tested specimen was 1.52 m long, 1.43 m wide, and 0.28 m deep. An actuator applied vertical loads at the center of the back skin of the specimen, resulting in a displacement of 158.7 mm and an ultimate load of 153.46 kN. Using these testing data, generation and calibration of a FE model of the tested specimen were executed in ABAQUS, indicating that the difference in the ultimate load between the calibrated model simulation and full-scale testing was only 3.32%. Then, six different DSs were simulated where the areas of the welded connection in the calibrated model were diminished for the DSs. It was found that the corners at the back skin-frame joint were prone to connection failure for all the DSs, and failure of the back skin-frame connection occurred remarkably from the distant edges.

Keywords**—**Computational analysis, damage scenarios, electronic road signs, finite element, welded connections.

I. Introduction

ELECTRONIC road signs have been effectively adopted as a roadside communication device by transportation authorities to convey messages on-road use to drivers, although these signs may also be used to convey a wide variety of real-time information such as the current weather, traffic conditions ahead, safety alerts, and so on [1]. Electronic road signs have been conventionally constructed using welded connections of several aluminum members and are still often the preferred connection method by many manufacturers [2]. Welding is an efficient connection type considering the short amount of time needed for serviceability from production. Another benefit of welding is that it can be performed at a wide range of temperatures and weather conditions. In spite of such benefits, however, failure in welds at different locations as well as the frame was observed in a study conducted with full-scale testing of a welded electronic road sign panel [3]. The experimental results seem to need an extended investigation of the failure modes of the panel to better understand their structural performance. FE modeling and simulations of the tested panel can also effectively reduce considerable time and effort in analyzing its failure behavior with differing damage conditions.

FE methods have been in use for nearly five decades for simulations of the mechanical behavior in welding [4] while development in this sector has been going on with newer findings. Due to the complexity of the structural behavior of welded connections under loads, numerous approaches for computational studies of welding connections were proposed [4]-[13]. Meanwhile, ABAQUS provides the option of a cohesive zone (e.g., cohesive-contact or elements) that can simulate the behavior of connections, including welding, adhesive, and so on, and multiple studies [10]-[13] have applied this option. In particular, Peng et al. [10] proposed a cohesive interface, which can assess weld connections in the design of modular structures subjected to wind, seismic, and/or gravity loads. For the proposed cohesive interface, two parameters, cohesive strength and critical separation of welding were sufficient to simulate the cohesive behavior of welding connection, while calibration of the proposed cohesive interface was fulfilled based on the experimental results of a compact tension test of steel weld joints conforming to ASTM E1820 [14]. A relatively slight error within 2% was observed between the experimental results and the FE model developed based on the proposed cohesive interface.

This study aims to assess the structural performance of an electronic road sign with welded connections using a FE model in ABAQUS [15] and analyze their failure patterns. Calibration of the FE model was carried out based on the results from full-scale testing of the electronic road sign subjected to ultimate loading. Including the current section, there are a total of six sections in this paper. In the following section, the full-scale testing of the electronic road sign and relevant results are described. The generation of a FE model and its calibration using available testing results are explained in the third and fourth sections, respectively. Using the calibrated FE model, parametric studies for various DSs were carried out in the fifth section. Findings from this study are summarized in the last section.

II. Testing Data

To evaluate the structural performance of welded aluminum connection in the electronic road sign, full-scale testing [3], [16], [17] was performed as shown in Fig. 1. The fabricated electronic road sign consisted of a frame, back skin, and two channels. The frame and channels were made of 6061 aluminum, while the back skin was made of 5052 aluminum. The frame and back skin were connected by welding, while the

Junwon Seo, PhD, PE is an associate professor in Department of Civil and Environmental Engineering at South Dakota State University, Brookings, SD 57007 USA (corresponding author, e-mail: junwon.seo@sdstate.edu).

Bipin Adhikari and Euiseok Jeong are graduate students in Department of Civil and Environmental Engineering at South Dakota State University, Brookings, SD 57007 USA (e-mail: bipin.adhikari@jacks.sdstate.edu, Euiseok.Jeong@sdstate.edu).

frame and the channels were connected using bolts as depicted in Fig. 1. The electronic road sign was 1.43 m wide (east to west), 1.52 m long (north to south), and 0.28 m deep. The system of this electronic road sign is installed vertically in field conditions where it is exposed to wind loads, acting prominently on the back skin. To simulate such conditions, the electronic road sign was flipped and installed on concrete abutments during the testing and loads were applied at the center of the back skin through an actuator as displayed in Fig. 1. Two steel I-beams were connected to the channels of the sign panel using bolts and the I-beams were rested on the concrete abutment to avoid any other influence than actuator load on the specimen. During the full-scale testing [3], the ultimate load was measured to be 153.46 kN at 158.57 mm displacement through the actuator.

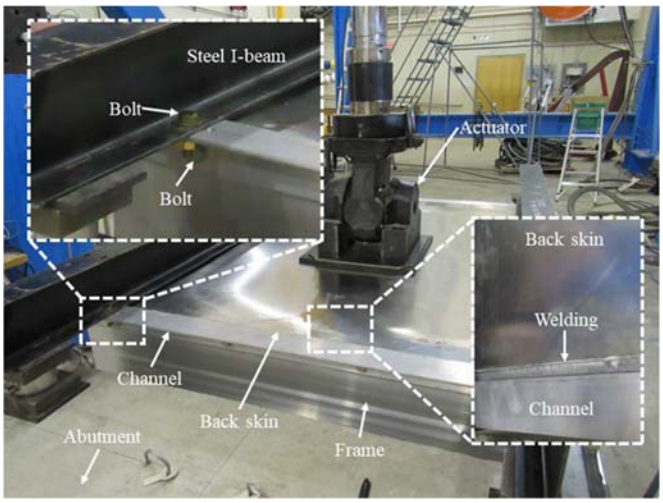

Fig. 1 Full-scale testing of an electronic road sign panel

III. FE Modelling and Simulation

A FE model of the tested electronic road sign panel was developed in commercial analysis software, ABAQUS [15] to perform simulations of loads acting on it. The FE model (refer to Fig. 2) was generated by combining the frame, back skin, weld filler, and two channels. Continuum 3-Dimensional 8-Node Reduced integration (C3D8R) among the available solid elements in ABAQUS was applied to the model, and the developed model consisted of a total of 18,013 C3D8R elements. Compared to Continuum 3-Dimensional 8-Node (C3D8), C3D8R shows a less expensive computational cost due to a relatively lower number of integration points, but the accuracy of C3D8R in the computational analysis is generally considered lower than C3D8. However, if a form of bending such as three-point is dominant, C3D8 tends to overestimate the ultimate load [12] and since bending is dominant in the referenced full-scale testing, the C3D8R is considered to be a more suitable element type for this study. Material properties (elastic modulus and shear modulus) of aluminum alloys (refer to Table I) were referred from the American Society for Metals (ASM) International [18] and Aerospace Specification Material Inc. [19], [20]. For the weld filler, 4043 weld filler was used, and the property values measured in a past study of small-scale testing [21] were applied as the properties of that filler, provided in Table I.

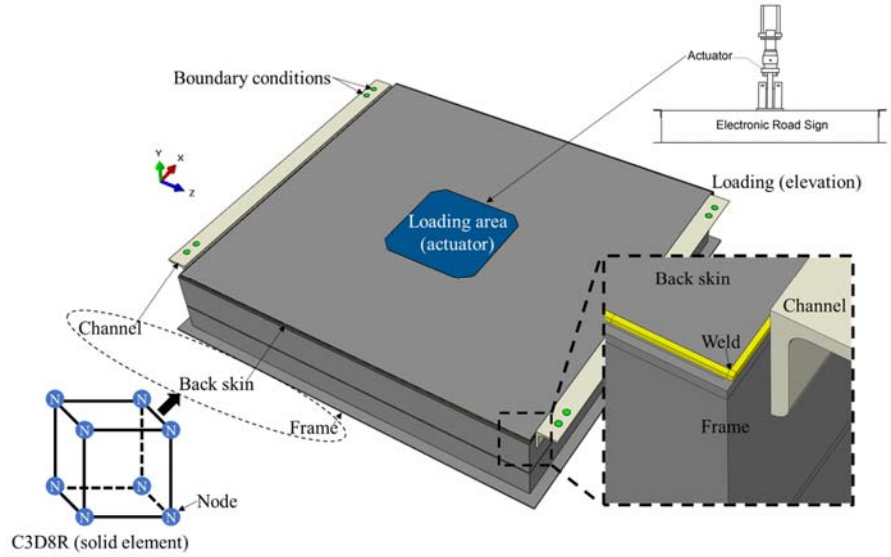

Fig. 2 FE model generation

Each of the created frames, back skin, channels, and weld fillers were combined by applying hard contact, tie constraint, and cohesive contact in ABAQUS. The tie constraint was applied to the bolt connection area, which exists between the frame and channels. As the bolted connection between the channels and the frame did not fail during the full-scale testing,

tie constraint was considered for that type of connection, while hard contact was applied to the contact surface except the bolt connection area. The reason behind it is that hard contact does not allow penetration between elements, and stress does not occur until contact occurs between the elements. The frame and back skin were connected by weld filler in the full-scale testing. To simulate this connection, the weld filler and the frame/back skin were connected by cohesive contact of ABAQUS [15] and hard contact was applied to all remaining surfaces, where the frame and the back panel were in contact. Cohesive contact is considered a suitable contact option to simulate the bonds involving welding, adhesive, and so on [10], [13], [22]. In addition, damage propagation and failure of welding due to loads in the joint can be simulated through the damage option of cohesive contact in ABAQUS. In this study, the maximum strength of the weld filler was applied through tensile strength and shear strength in the damage option.

TABLE I
MATERIALS

Parts	Models	Elastic modulus	Shear modulus
Frame	6061 aluminum	68.9 GPa	26.0 GPa
Back skin	5052 aluminum	70.3 GPa	25.9 GPa
Channels	6061 aluminum	68.9 GPa	26.0 GPa
Weld fillers	4043 weld filler	87.3 GPa	49.9 GPa

As shown in Fig. 2, boundary conditions were set according to the area (light green areas in Fig. 2) of the steel I-beam and these boundary conditions simulated bolt connections in full-scale testing. During the full-scale testing, movement of the steel I-beam was restricted and its connection with the frame was fixed. The fixed boundary conditions were applied where displacement did not occur (green areas in Fig. 2) in the length, height, and width directions as in the full-scale testing. Boundary conditions were applied to the FE model before the occurrence of any external force. With the appropriate boundary conditions applied, at first gravity loads were applied to the entire model to simulate the testing set-up. After all gravity loads were considered, a displacement of 158.57 mm (measured at the ultimate load from the full-scale testing) was applied to the center of the back skin of the FE model.

IV. Calibration Using Testing Data

To calibrate the developed model, the load-displacement data obtained from the FE model were compared with those gained from the full-scale testing as depicted in Fig. 3. From this figure, it can be observed that the full-scale testing data and the overall trend of the FE model are similar. The calibrated FE model showed an ultimate load of 148.51 kN at the applied displacement of 158.57 mm. In particular, this value showed an extremely slight difference of 3.32% compared to the result of full-scale testing. Note that a gentle decrease in the load can be observed when displacement in the FE model went from 61 mm to 81 mm. This decrease in load was considered to be induced by the failure of welded connection between the back skin and the frame. The further testing and FE analysis data in Fig. 3 are obtained from Amatya et al. [3], [16], [17].

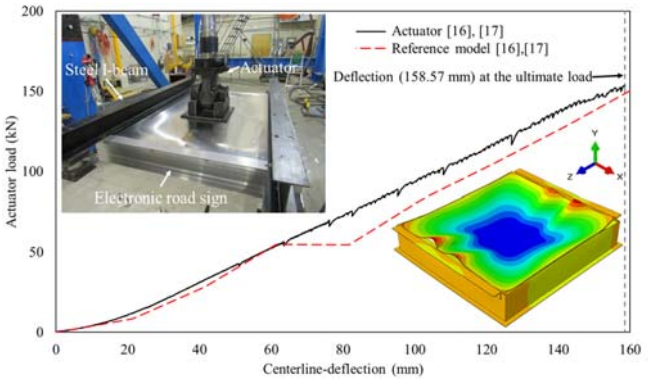

Fig. 3 The ultimate load of specimen and reference model

V. Damage Scenarios

Supplemental DS models were developed based on the calibrated model which is used as a reference model (RM). An analysis was carried out considering the reduction of welding coverage in the cardinal directions of the model to simulate an inappropriate condition such as poor-quality welding or imbalances of applied external forces. A total of six scenarios (i.e., DS 1 through DS 6) were developed as provided in Table II. The reductions in weld connection coverage were considered comparing to the coverage provided in the RM. For example, DS 1 assumed that 33% of the total length of welding on the west side was defective, whereas DS 2 considered a reduction of 33% for welding on the east side. Fig. 4 shows load-displacement curves of the actuator load from the full-scale testing, the RM, and six DS models. 33% reduction in west side weld connection (DS 1) and 33% reduction in east side weld connection (DS 2) showed only 0.23% and 0.38% reductions in the ultimate load, respectively, compared to the RM. On the other hand, welding coverage reduction in all four directions (DS 5) and 100% reduction in welding coverage for the north and south edges (DS6) showed significant ultimate load reductions of 38.46% and 52.98%, respectively. Table II provides the values of welding coverage reduction and the corresponding ultimate load for each scenario, where percentage differences in the ultimate loads of DSs in comparison to the RM are provided in parentheses in Table II.

TABLE II
STUDIED DSs

	Connection Reduction				Ultimate Load[a]
Model	North	South	East	West	
Actuator	—	—	—	—	153.46 kN
RM	—	—	—	—	148.51 kN
DS 1	—	—	—	33%	148.18 kN (0.23%)
DS 2	—	—	33%	—	147.94 kN (0.38%)
DS 3	—	50%	33%	—	115.56 kN (22.19%)
DS 4	50%	—	—	33%	113.69 kN (23.45%)
DS 5	50%	50%	67%	67%	91.40 kN (38.46%)
DS 6	100%	100%	—	—	69.86 kN (52.98%)

[a]Numbers in parentheses indicate percentage differences in the ultimate loads compared to the RM.

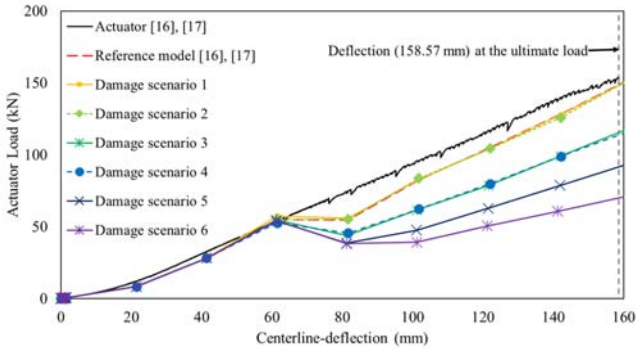

Fig. 4 Load-displacement according to DSs

Figs. 5 and 6 show representative failure patterns of the FE models immediately after a displacement of 158.57 mm was reached at the center of the back skin for DS 1 and DS 6, respectively. The contour in the figure is set to display different colors in the members according to its respective displacement (rainbow gradient). When maximum displacement in the positive direction occurs, the displayed color is red, whereas the region with the maximum displacement in the negative direction is displayed in navy. Note, the channels are set to not be visible after the analysis because welding connections are not applied to them. Fig. 5 shows the behavior of the FE model of DS 1, where in contrast to the deflection of the center of the back skin, a camber measuring up to 46.98 mm on the outside of the back skin along two edges is observed (see Fig. 5 (a)). This phenomenon is observed as a result of an external force exceeding the maximum stress of the cohesive contact with the weld connecting the back skin and the frame occurred (weld failure). In Fig. 5 (b), a total of eight distortions of the back skin were found–four distortions at the corner and two distortions each at the north (see Fig. 5 (c)) and south (see Fig. 5 (d)) edges, whereas weld failure on the east (see Fig. 5 (e)) and west (see Fig. 5 (f)) edges were not observed. It is considered that the effect of greater shear/tension force on the north and south edges occurred due to the model/specimen being 9 cm longer in that direction compared to the east and west edges.

For the DS 6's FE model immediately after the application of the same displacement of 158.57 mm on the back skin, a camber measuring up to 86.13 mm on the back skin was observed, as shown in Fig. 6 (a). This is an 83.33% increase compared to the 46.98 mm camber measured in DS 1 (Fig. 5). In Fig. 6 (b), a total of six distortions of back skin can be observed. As opposed to DS 1, only one central deformation was found on the north (refer to Fig. 6 (c)) and south (refer to Fig. 6 (d)) edges each, whereas, similar to DS 1, deformation was observed in all four corners of the back skin. No deformation was observed in the east (refer to Fig. 6 (e)) and west (refer to Fig. 6 (f)) edges. For DS 1 and DS 6, significant welding failures on north and south edges were observed, but different damage patterns were observed. In the analysis of DS 1, two significant distortions were detected on each of the north and south edges where welding connection lying between distortions had not failed, whereas only one significant distortion on north and south edges was identified in the analysis of DS 6. Similarly, failure patterns resulting from the other DS models are in agreement with those shown in DS 1 and DS 6 models.

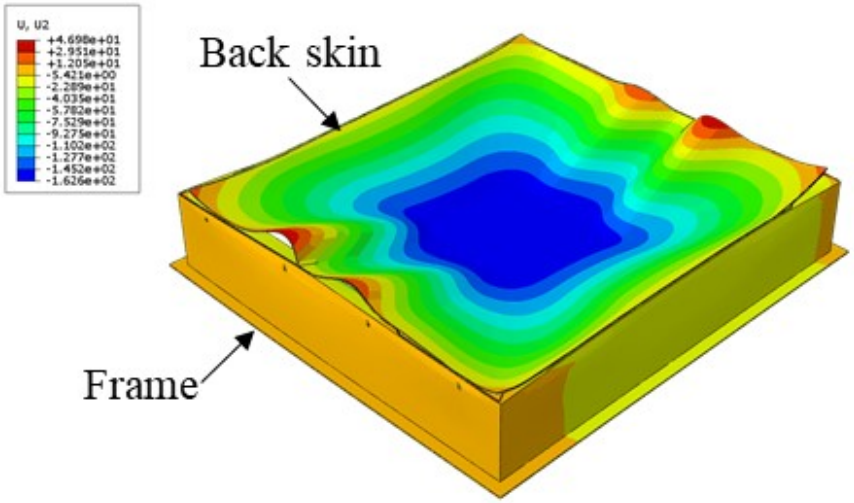

(a)

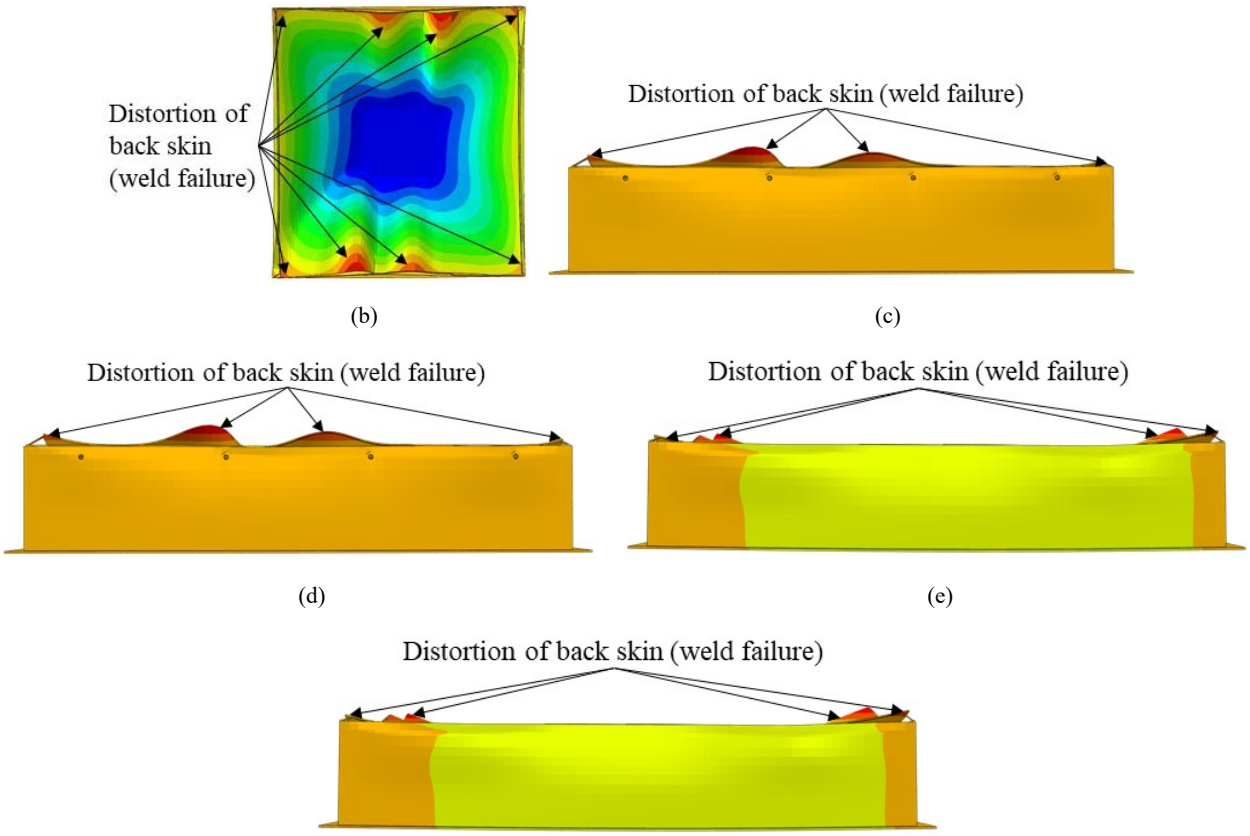

Fig. 5 Failure patterns of DS 1 model at the ultimate load: (a) isometric view; (b) plan view; (c) north side; (d) south side; (e) east side; and (f) west side

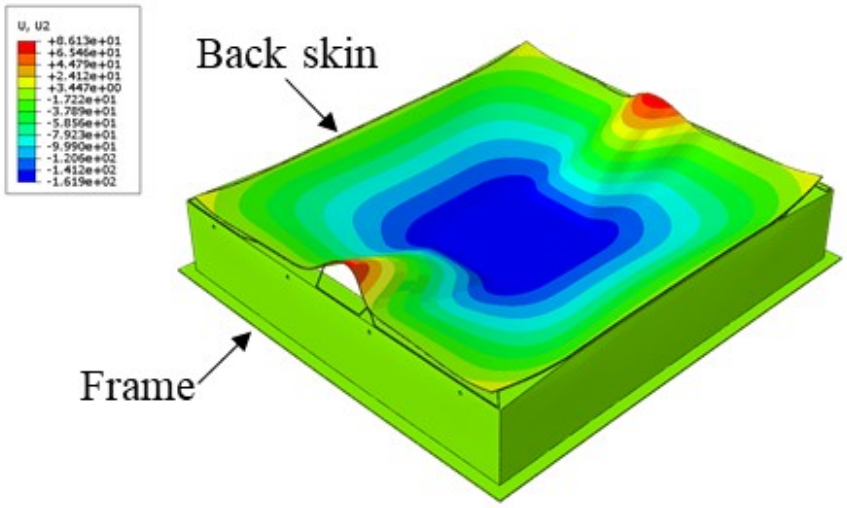

(a)

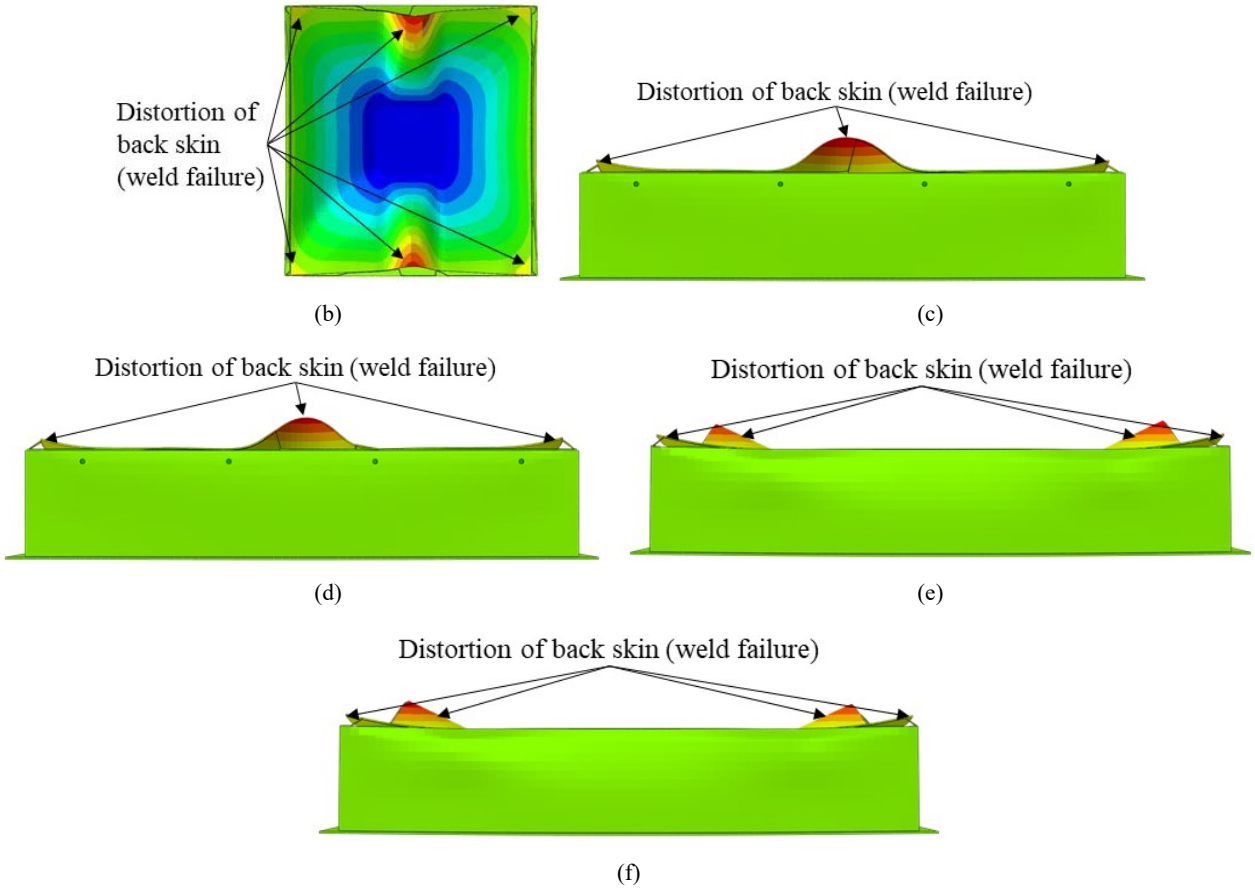

Fig. 6 Failure patterns of DS 6 model at the ultimate load: (a) isometric view; (b) plan view; (c) north side; (d) south side; (e) east side; and (f) west side

VI. Conclusion

This study was intended for the computational analysis of the damage pattern observed for welded aluminum electronic road sign panels through FE modeling and simulations. A reference FE model was developed in FE software ABAQUS and calibrated with the results of a full-sized electronic road sign panel tested in the laboratory. The calibrated RM had a similar load carrying capacity as compared to the full-scale testing specimen, based on which computational studies through simulations were carried out to investigate the patterns of damage occurring due to differential coverage of welded joints. A parametric study was conducted with six different DSs and results on the reduction of ultimate loads were obtained. The following conclusions were drawn based on the results of the parametric study.

1) For all DSs, loads increased in the same pattern when the deflection in the back skin increases from 0 mm to 61 mm. Loads for DSs at 61 mm deflection fell within a range of 52.62 kN and 59.85 kN, from where a gentle decrease was observed for deflection up to 81 mm for DS 1 to DS 6. This range of deflection was where the welding failure occurred in the DS models. For the RM and DS1, the observed load reduction at welding failure was similar.
2) Reduction in weld coverage along the east and west edges of the road sign by 33% insignificantly reduced the overall load-carrying capacity of the sign panel. The load was reduced by only 0.23% and 0.38%, respectively, compared to the RM. A significant loss of loads occurred more prominently when welded connections on the north and south edges were reduced.
3) In the simulations of all the DS models, significant distortions at all the four corners and the north and south edges were observed. For DS 6, particularly, a total of six distortions of back skin occurred because the ultimate load appeared to be dependent upon the coverage areas of the welded connection on the shorter edges.

Acknowledgment

The contents of this paper reflect the views of the authors, who are responsible for the facts and accuracy of the data presented herein. Any opinions, findings, conclusions, or recommendations expressed in this publication are those of the authors.

References

[1] Tay, R., and A. G. de Barros. Public Perceptions of the Use of Dynamic Message Signs. *Journal of Advanced Transportation*, Vol. 42, No. 1, 2008, pp. 95–110. https://doi.org/10.1002/atr.5670420107.
[2] Amatya, I., J. Seo, E. Jeong, and J. Lee. Numerical Study for Structural Performance Evaluation of Adhesively Bonded Aluminum Dynamic Message Signs. *Thin-Walled Structures*, 2020, p. 107193.

https://doi.org/10.1016/j.tws.2020.107193.

[3] Amatya, I. *Structural Performance Evaluation of Dynamic Message Signs with Adhesive and Welded Joints*. Electronic Theses and Dissertations. 4067. South Dakota State University, Brookings, SD, 2020.

[4] Anca, A., A. Cardona, J. Risso, and V. D. Fachinotti. Finite Element Modeling of Welding Processes. *Applied Mathematical Modelling*, Vol. 35, No. 2, 2011, pp. 688–707. https://doi.org/10.1016/j.apm.2010.07.026.

[5] Sadigh, M. A. S., G. Marami, and B. Paygozar. Failure Simulation in Resistance Spot-Welded Lap-Joints Using Cohesive Zone Modeling. *Journal of Central South University*, Vol. 25, No. 11, 2018, pp. 2567–2577. https://doi.org/10.1007/s11771-018-3936-z.

[6] Cavalli, M. N., M. D. Thouless, and Q. D. Yang. Cohesive-Zone Modelling of the Deformation and Fracture of Spot-Welded Joints. *Fatigue & Fracture of Engineering Materials & Structures*, Vol. 28, No. 10, 2005, pp. 861–874. https://doi.org/10.1111/j.1460-2695.2005.00919.x.

[7] Guishen, Y., C. Xin, and W. Zitao. Effect of Adhesive Ductility and Joint Configuration on the Tensile-Shear Behaviors of Friction Stir Spot Weld Bonding Joints. *The Journal of Adhesion*, 2021, pp. 1–24. https://doi.org/10.1080/00218464.2021.1932484.

[8] Palmonella, M., M. I. Friswell, J. E. Mottershead, and A. W. Lees. Finite Element Models of Spot Welds in Structural Dynamics: Review and Updating. *Computers & Structures*, Vol. 83, No. 8, 2005, pp. 648–661. https://doi.org/10.1016/j.compstruc.2004.11.003.

[9] Wang, T., O. S. Hopperstad, P. K. Larsen, and O.-G. Lademo. Evaluation of a Finite Element Modelling Approach for Welded Aluminium Structures. *Computers & Structures*, Vol. 84, No. 29, 2006, pp. 2016–2032. https://doi.org/10.1016/j.compstruc.2006.08.011.

[10] Peng, J., C. Hou, and L. Shen. Numerical Simulation of Weld Fracture Using Cohesive Interface for Novel Inter-Module Connections. *Journal of Constructional Steel Research*, Vol. 174, 2020, p. 106302. https://doi.org/10.1016/j.jcsr.2020.106302.

[11] Deng, D., H. Murakawa, and W. Liang. Numerical Simulation of Welding Distortion in Large Structures. *Computer Methods in Applied Mechanics and Engineering*, Vol. 196, No. 45, 2007, pp. 4613–4627. https://doi.org/10.1016/j.cma.2007.05.023.

[12] Selamet, S., and M. Garlock. Guidelines for Modeling Three Dimensional Structural Connection Models Using Finite Element Methods. Presented at the International symposium: steel structures: culture & sustainability, Istanbul, Turkey, 2010.

[13] Shim, D.-J., D. Rudland, and F. Brust. Comparison of Through-Wall and Complex Crack Behaviors in Dissimilar Metal Weld Pipe Using Cohesive Zone Modeling. Volume 6A: Materials and Fabrication, 2013.

[14] ASTM E1820-20b. *Standard Test Method for Measurement of Fracture Toughness*. ASTM International, West Conshohocken, PA, 2020.

[15] ABAQUS. *ABAQUS 6.14: User's Manual*. Dassault Systemes Simulia Corporation, RI, USA, 2014.

[16] Amatya, I., J. Seo, and E. Jeong. Computational Parametric Study on Full-Scale Ultimate Tested Dynamic Message Sign with Welded Connections. *Journal of Structural Engineering, In Review*, 2021.

[17] Seo, J., and I. Amatya. Structural Performance of Dynamic Message Signs with Adhesive and Welded Connections. *Engineering Structures, In Review*, 2021.

[18] American Society for Metals (ASM) international. *6061-T6 Aluminum Alloy Sheet, Compressive Stress-Strain Curves*. ASM international, Russell Township, OH, 2002, p. 188.

[19] Aerospace Specification Material Inc. Aluminum 5052-H32. http://asm.matweb.com/search/SpecificMaterial.asp?bassnum=MA5052H32. Accessed Dec. 2, 2019.

[20] Aerospace Specification Material Inc. Aluminum 6061-T6; 6061-T651. http://asm.matweb.com/search/SpecificMaterial.asp?bassnum=MA5052H32. Accessed Dec. 2, 2019.

[21] Seo, J., I. Amatya, T. Letcher, and E. Jeong. Welding versus Adhesive Bonding Strength Investigation. *Engineering Failure Analysis, In Review*, 2021.

[22] Woelke, P. B., B. K. Hiriyur, K. Nahshon, and J. W. Hutchinson. A Practical Approach to Modeling Aluminum Weld Fracture for Structural Applications. *Engineering Fracture Mechanics*, Vol. 175, 2017, pp. 72–85. https://doi.org/10.1016/j.engfracmech.2017.02.010.